SINGLE-SHOT PULSED DETONATION DEVICE FOR PDE COMBUSTION SIMULATION

Carla S. T. Marques, carlatm@ieav.cta.br
Antonio C. de Oliveira, acoc@ieav.cta.br
Aerothermodynamic and Hypersonic Division, Institute of Advanced Studies – Department of Aerospatial Science and Technology, Rodovia dos Tamoios, km 5.5, 12228-001 São José dos Campos – SP, Brazil

Fernando B. Dovichi Filho
William C. Ferraz
Aerothermodynamic and Hypersonic Division, Institute of Advanced Studies – Department of Aerospatial Science and Technology, Rodovia dos Tamoios, km 5.5, 12228-001 São José dos Campos – SP, Brazil

José B. Chanes Jr., brosler@ieav.cta.br
Aerothermodynamic and Hypersonic Division, Institute of Advanced Studies – Department of Aerospatial Science and Technology, Rodovia dos Tamoios, km 5.5, 12228-001 São José dos Campos – SP, Brazil

Abstract. *In this work, a single-shot pulsed detonation device for experimental simulation of the PDE combustion conditions in supersonic and hypersonic flight regimes ($M_\infty \leq 6$) is proposed. The combustion device is composed of: ignition system, detonation tube without obstacles, divergent nozzle and test chamber. A nanosecond spark discharge has been developed to promote a direct detonation initiation or a DDT in the shortest distance possible. Pulses of approximately 25, 65 and 80 ns (FHWM) were acquired. Emission and Schlieren images were taken to characterize the spark discharge. The pulsed detonation device was planned to achieve typical specific impulse (Isp ≈ 200s) for a single-shot PDE. 1-D calculations were performed to establish the combustion conditions for experimental tests. Flight conditions between 0 and 20,000 m of altitude fueled with H_2/air and C_2H_4/air mixtures were calculated within 0.5-1.5 atm range of initial pressure at different equivalence ratios for two nozzle area ratios. The nozzle exit velocities are notably higher if mean pressure of PDE cycle (P_{mean}) is considered. Assuming mean pressures of PDE cycle, experimental conditions with Mach number (M_x) from 3.0 to 3.7 can be simulated for these explosive mixtures. The results show PDE flight regimes from transonic to supersonic. However, it is promising to reach higher pressures and velocities through the ignition system proposed and, consequently hypersonic flight regimes.*

Keywords*: nanosecond discharge, Thyratron, detonation, PDE, scramjet.*

1. INTRODUCTION

Pulsed detonation engines (PDEs), in recent decades, have been developed due to their high potential application as an aerospace propulsion system across subsonic, supersonic and hypersonic flight regimes (Tangilara *et al*, 2005). There are wide applications for these devices, but the most promising is the scramjet development (Povinelli, 2002; Falepim *et al*, 2001; Cambier *et al*, 1995), which will allow easy access to space.

The thermodynamic advantage of detonations in front of deflagrations processes, which provide high specific impulse in a broad range of Mach number, the reduced complexity and the lower operational cost became PDEs very attractive (Kailasanath, 2003) and nowadays they are a real possibility as aircraft engines (FlightGlobal, 2008). However, reliable and repeatable detonations in the shortest distance possible are required to achieve a practical PDE; and the key to make this feasible is the detonation initiation (Lee *et al*, 2005; Zhukov *et al*, 2006).

Detonations can be initiated through two different ways: a slow mode where there is a deflagration-to-detonation transition (DDT) and a fast mode generated by a powerful ignition or a strong shock wave. Sometimes, they are designated as auto-ignition (or thermal initiation) and direct ignition, respectively (Marques, 1996). Direct initiation of hydrocarbon propellant detonation demands high-energy input of kilojoules magnitude (Lee *et al*, 2000; Zhukov and Starikovskii, 2006). Deflagrations that auto-propagate are intrinsically instable and accelerate continuously after ignition. Under appropriate conditions, they can accelerate to high supersonic velocities and abruptly transit to detonations. However, the reaction zone propagates very differently than those ignited by shock waves (Lee, 2008).

Wintenberger and Shepherd (1999) have reported the mechanism of intensifying a shock wave by coherent energy release (SWACER mechanism) as the most effective method for accelerating a deflagration-to-detonation transition, through a quasi homogeneous field of radicals in a gas using a spatially homogeneous discharge of short duration. Nanosecond discharge ignition has been shown as a high-velocity ionization wave with spatial homogeneity and small times of gas excitation, which is dominated by reactions of direct dissociation of the gas and dissociative extinction with great contribution to the pool of active species (Starikovskii, 2003; Zhukov and Starikowskii, 2006).

In this work, a single-shot pulsed detonation device for experimental simulation of the PDE combustion conditions in supersonic and hypersonic flight regimes ($M_\infty \leq 6$) is proposed. A high-voltage nanosecond spark discharge has been developed and experimentally characterized with aim to promote a direct detonation initiation or a small length and

time of DDT. Unidimensional calculations were performed to establish the detonation and flight conditions for experimental trials.

2. PULSED DETONATION DEVICE

The single-shot pulsed detonation device is composed by an ignition system, a detonation tube without obstacles, a divergent nozzle and a test chamber. A diaphragm will isolate the explosive mixtures in the detonation tube from other device's parts under vacuum. Both detonation tube and test chamber will be equipped with optical windows and piezoelectric pressure sensors. Figure 1 shows a diagram of the device.

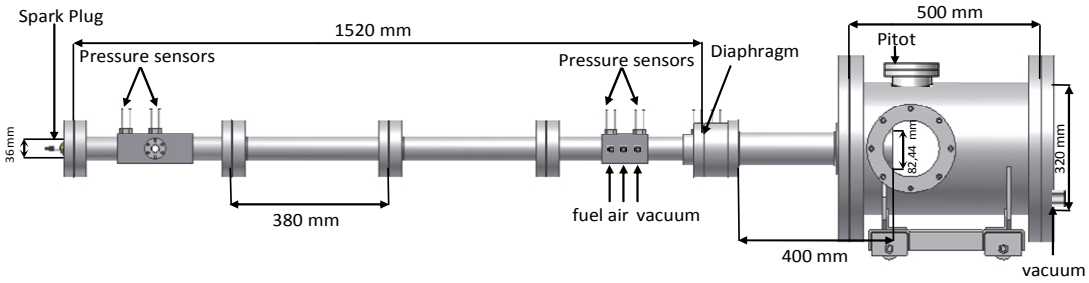

Figure 1. Single-shot pulsed detonation device.

The detonation chamber and nozzle dimensions were planned based on literature data (Dryer *et al*, 2003; Kailasanath, 2003; Kasahara *et al*, 2002; Bertran *et al*, 1998). The device was dimensioned for L/D = 42 (tube length/tube diameter ratio) and β = 0.16-0.26 (nozzle length/tube length) to achieve typical specific impulse (Isp ≈ 200s) for a single-shot PDE. Expansion ratios (AR = 5.2 and AR = 11.0) next to the optimal for high specific impulses (AR = 4.0 and AR = 11.0) of PDE were applied.

3. IGNITION SYSTEM

An ignition system by discharge of short duration using an automotive spark plug has been developed to accelerate a DDT or to reach a direct initiation without the need of obstacles inside the tube, as Shchelkin spiral. The obstacles increase gas mixing and produce local inhomogeneities for accelerating the combustion, but this depends on the initial deflagration velocity and, further, reduces the specific impulse (Zhukov and Starikovskii, 2006). High-voltage nanosecond discharge seemed to be a good alternative method, since it is a highly effective means of production of active species with high spatial homogeneity in a short time. In this way, some circuits for nanosecond discharge with different spark plugs were tested for PDE ignition purposes.

3.1. High-voltage pulse generator

The high-voltage pulse generator is similar to discharge circuit of CO_2 and N_2 lasers, which are switched by a Thyratron. The basic circuit of discharge consists of a high-voltage supply to charge a capacitor of 75 nF, a fast switch (Ceramic Metal Deuterium Thyratron, HY3003) to drive the short time discharge at spark plug and a resistor of 100 kΩ that enabled the changes in the circuit to reach different pulse widths. Figure 2 shows a circuit diagram for nanosecond discharge. High-voltages pulses from three different circuits were temporally characterized by voltage and current: (a) circuit without L1 and C2; (b) circuit with L1 = 2 μH and C2 = 3.6 nF and (c) saturable L1of 175 μH and C2 = 3.6 nF (Fig. 2) through a digital oscilloscope (Yokogawa, DL 7480). Energies of 15-34 J and voltages of 20-30 kV were applied at different automotive spark plugs (BP5ES and BP5ET from NGK).

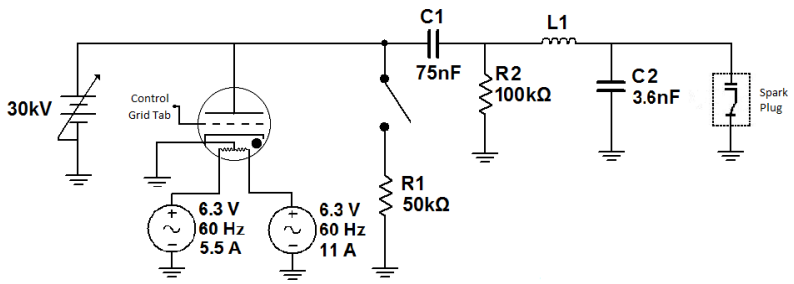

Figure 2. Circuit diagram for nanosecond discharge.

3.2. Emission images

Emission images from nanosecond discharge were detected with an intensified coupled-charge device (ICCD) camera (Cooke instruments, DICAM Pro) for visualization of the production of active species. The optics imaging consisted of Nikon fused-silica lens with relative aperture of f/5.6. An interference filter (Melles Griot, F10-310.0-3) centered at 310 nm (FWHM = 10 nm) was applied to UV images. It allows properly select the light emission mainly from OH radicals ($A^2\Sigma^+ - X^2\Pi$), O-atoms ($^4P_{5/2} - {}^4D^0{}_{7/2}$, $^4P_{3/2} - {}^4D^0{}_{5/2}$) and slightly O_2 molecules ($B^3\Sigma_u^- - x^3\Sigma_g^-$). All these species can be generated through discharge. A home-made delay generator was used for time synchronism of the ICCD camera and high-voltage pulse of the nanosecond discharge. The delay time of the ICCD camera was set to acquire images from peak voltage and gate widths of 30 ns and 60 ns were used dependent on detection request. The sensitivity of the MCP image intensifier was adjusted at 80%.

UV emission images of three different high-voltage pulse widths of the nanosecond discharge for standard and supplementary gap spark plugs under 1 atm of air were obtained. High-voltages of 20 and 25 kV were applied to generate the discharge. All images were normalized by calculation code developed in Mathcad software by our group for image processing. Visible images of spark plugs were also taken with a neutral density filter (OD = 3.0) to identify the ground and central electrodes, and help in image analysis.

3.3. Schlieren images

The conventional Schlieren measurements were also applied for visualization of the shock wave appearance with our nanosecond discharge, in a way similar to those usually adopted by our group (Oliveira *et al*, 2008). Systematic measurements as for emission images were carried out. The Schlieren system consisted of a xenon flash lamp, two parabolic mirrors, a knife edge (razor blade) and an ultra high-speed digital framing camera (Cordin, 550). The camera was set to 200,000 fps for imaging of the nanosecond discharge effect on air. A multichannel time-delay generator was used to synchronize the flash lamp, the high-speed camera and the high-voltage pulse of the nanosecond discharge. All images were acquired with a camera delay time of 112 μs.

4. CALCULATIONS

Unidimensional calculations were carried out to determine the detonation and expansion parameters for experimental tests in the pulsed detonation device of V_{tube} = 1.55 dm^3. Chapman-Jouguet (CJ) ideal detonation conditions were calculated through CEA/NASA software. Taylor expansion was applied to the detonation products and the mean pressure of PDE cycle was investigated since it is able to simulate more reliable specific impulse. Steady isentropic flow was assumed for nozzle expansion. The steadily-propagating detonation model considers four regions: stationary reactants ahead of detonation mixture (state 1); the detonation wave between states 1 and 2 (jump condition); the expansion wave behind the detonation (between states 2 and 3) and the stationary products (state 3). The detonation travels at a constant velocity, D_{CJ} and the peak pressure is P_2 or P_{CJ} (Browne *et al*, 2004). The detonation products in the state 3 are the nozzle inlet flow to be expanded. Two choices for expansion to the sonic point (nozzle inlet) were made, Taylor expansion pressure (P_3) and mean pressure of a PDE cycle ($\overline{P}$). The mean pressure was calculated for states 2 and 3, since they are the contributors for cycle-mean thrust (Roy *et al*, 2004, Cooper and Shepherd, 2004). Standard equations of ideal and steady flow for detonation tubes with nozzles were used (Browne *et al*, 2004, Cooper and Shepherd, 2004). Table 1 shows the nomenclature for equations used and physical quantities calculated.

Table 1. Nomenclature for physical quantities.

Nomenclature	
AR = nozzle area ratio	Px = static pressure in nozzle exit
c_{CJ}= CJ sound speed	P_o(amb.) = ambient pressure
c_3 = sound speed in Taylor expansion	P_o (flight) = flight pressure
c_x = sound speed in nozzle exit	q = Pitot pressure
D_{CJ} = CJ detonation velocity	T_1 = initial temperature
M_{CJ} = CJ Mach number	T_{CJ} = CJ temperature
M = nominal Mach number	T_3 = Taylor expansion temperature
Mx = Mach number in nozzle exit	$\overline{T}$ = mean temperature
M_∞ = flight Mach number	Tx = temperature in nozzle exit
P_1 = initial pressure	Ux = gases velocity in nozzle exit
P_{CJ} = CJ pressure	W(g/mol) = molar weight in detonation
P_3 = Taylor expansion pressure	Φ = equivalence ratio
$\overline{P}$ = mean pressure of PDE cycle	γ = specific heat ratio

5. RESULTS

5.1. Discharge experimental characterization

5.1.1. High-voltage pulses

High-voltage and current pulses of the nanosecond discharge with different circuits by applying 25 kV to charge the capacitor are presented in Fig. 3. They are practically equals for standard and supplementary gap spark plugs.

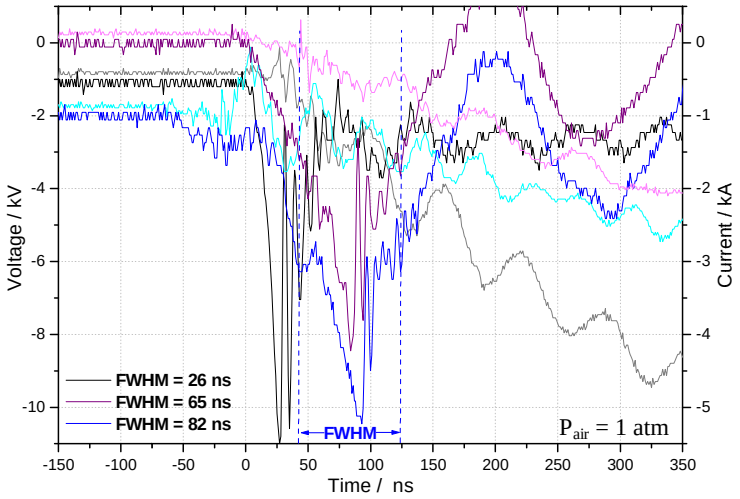

Figure 3. High-voltage and current pulses from different nanosecond discharge circuits by applying 25 kV. Black and gray lines – (a) circuit without L1 and C2; purple and magenta lines – (b) circuit with L1 = 2.4 μH and blue and cyan lines – (c) circuit with saturable L1 of 175 μH.

Peak voltages of 8.5 kV and peak currents of 4.0 and 4.5 kA were registered for nanosecond discharge with inductor and peaking capacitor: (b) and (c), respectively. Whereas, 10.0 kV and 5.5 kA were found for basic circuit of discharge. The initial time point of all pulses was placed at zero in x-axis. Pulses widths of 26, 65 and 82 ns for full width at half maximum (FWHM) were obtained for the discharge circuits tested.

5.1.2. Emission images

Figure 4 shows the emission images acquired for high-voltage pulses of the nanosecond discharge at spark plugs.

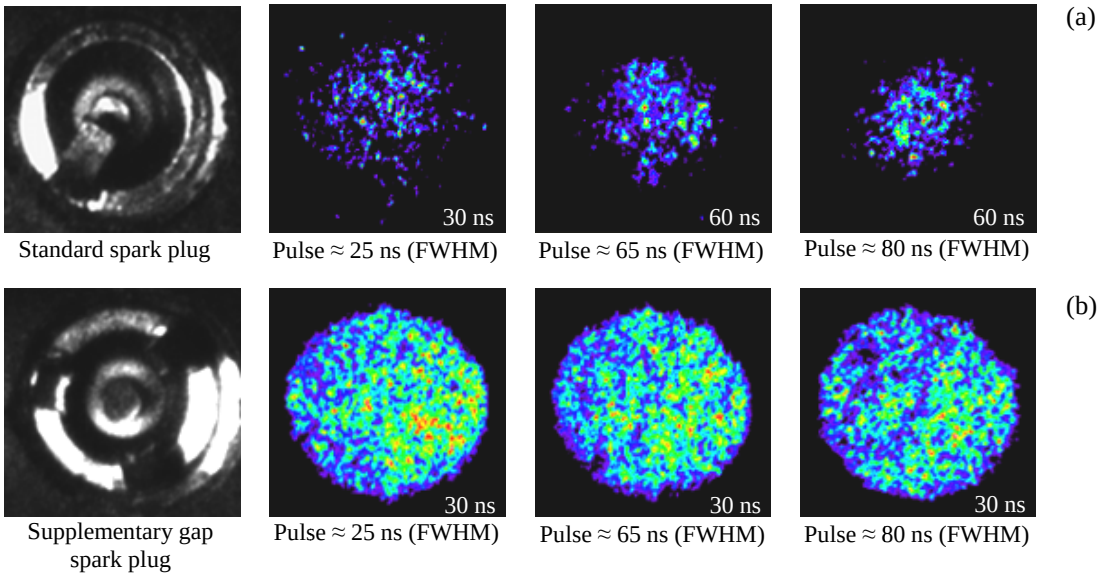

Figure 4. Visible and UV emission images from nanosecond discharge at (a) standard and (b) supplementary gap spark plugs under 1 atm of air. 25 kV was applied. Exposure time of each photograph was placed on images.

From emission images it is possible to identify a more intense discharge for supplementary gap than standard spark plug. Furthermore, they allow the visualization of the nanosecond discharge shape on the electrodes. For standard spark plug, there are strong luminescent points or high concentration of active species located next to the central electrode independent on pulse width. For the other spark plug, the discharge shape is clearly discernible as the circuit applied or resultant pulse width. There is a predominant production of active species on one of the three ground electrodes for high-voltage pulses with ca. 25 ns. While for pulses with ca. 65 and 80 ns, the active species are found in all of them. However, higher concentration and a more homogeneous distribution of active species are observed for high-voltage pulses of 65 ns. In addition, the radial discharge shape visualized by emission images taken for pulses of 65 ns point out the occurrence of streamer discharges or transient plasma (Shiraishi *et al*, 2009). Voltages of 20 and 25 kV were applied in discharge and the same effect was observed. The emission results show the high-voltage pulse of 65 ns at supplementary gap spark plug, probably, as the most efficient for ignition.

5.1.3. Schlieren images

Schlieren images from nanosecond discharge for visualization of shock wave appearance were taken as shown in Fig. 5.

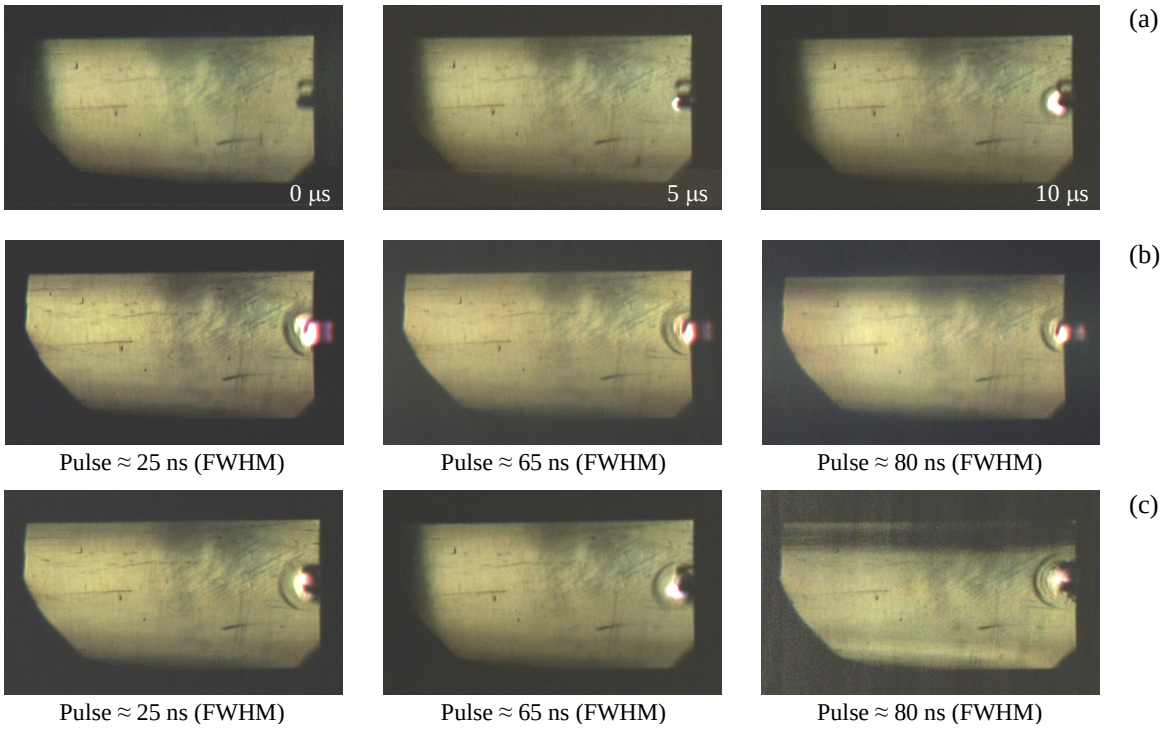

Figure 5. Schlieren visualization of the nanosecond discharge under 1 atm of air (a) shock wave time evolution; shock wave at different high-voltage pulses at (b) standard and (c) gap supplementary spark plugs.

Figure 5 (a) shows the shock wave time evolution, from which is evident that a planar shock wave appears within 5 μs after beginning of the nanosecond discharge. All discharge conditions studied generated shock waves, as shown through the images acquired after 10 μs of camera trigger in Figs. 5(b) and 5(c). However, the shock waves are slightly inclined in the direction of the ground electrode for discharge at standard spark plug, while they are perfectly semi-spherical developed at supplementary gap spark plug. Instabilities on detonation can be expected by applying a nanosecond discharge at standard spark plug due to angled shock wave. Therefore, a nanosecond discharge at supplementary gap spark plug is more suitable for detonation initiation. Energies above 15 J (20 kV) were enough to produce a shock wave.

The results from emission and Schlieren images reveal a promising ignition system for pulsed detonation engines, but experimental tests ought to carry out to verify a shorten DDT or a direct detonation.

5.2. PDE cycle calculations

Tables 2 and 3 show parameters of detonation cycle and nozzle expansion calculated for H_2/air and C_2H_4/air explosive mixtures within 0.5-1.5 atm range of initial pressure at different equivalence ratios. Nozzle expansion calculations for two area ratios were performed.

Table 2. Detonation cycle and nozzle expansion parameters for H_2/air explosive mixture.

H_2/air Explosive Mixture													**T_1 = 298 K**
CJ Detonation, Taylor Expansion and Mean Pressure of PDE cycle													
P_1 / atm	**Φ**	**P_{CJ} / atm**	**T_{CJ} / K**	**M_{CJ}**	**D_{CJ} / m s^{-1}**	**γ**	**c_{CJ} / m s^{-1}**	**P_3 / atm**	**T_3 / K**	**c_3 / m s^{-1}**	**$\bar{P}$ / atm**	**$\bar{T}$ / K**	
0.5	0.6	6.4	2414.1	4.43	1704.0	1.21	968.2	2.46	2038.1	889.6	4.45	2262.1	
0.5	0.8	7.3	2730.9	4.67	1853.1	1.17	1034.8	2.77	2361.1	962.2	5.01	2582.6	
0.5	1.0	7.7	2891.5	4.80	1953.5	1.16	1080.6	2.93	2535.3	1011.9	5.31	2749.3	
0.5	1.2	7.8	2920.0	4.82	2015.4	1.16	1116.4	2.95	2552.2	1043.7	5.36	2773.0	
0.5	1.4	7.7	2884.3	4.80	2056.2	1.17	1145.0	2.90	2497.9	1065.5	5.28	2729.5	
1.0	0.6	12.9	2423.8	4.44	1707.5	1.22	971.8	4.92	2039.5	891.4	8.90	2268.3	
1.0	0.8	14.6	2761.7	4.70	1862.7	1.18	1042.7	5.56	2375.1	967.0	10.09	2606.5	
1.0	1.0	15.6	2942.0	4.83	1968.5	1.16	1091.0	5.92	2567.8	1019.3	10.75	2792.5	
1.0	1.2	15.7	2969.0	4.85	2030.4	1.16	1127.5	5.95	2580.4	1051.1	10.82	2813.6	
1.0	1.4	15.4	2924.9	4.83	2069.2	1.18	1155.7	5.84	2516.7	1072.0	10.64	2761.3	
1.5	0.6	19.4	2428.7	4.44	1709.2	1.22	973.6	7.38	2040.1	892.3	13.37	2271.4	
1.5	0.8	22.0	2777.9	4.71	1867.7	1.18	1047.0	8.36	2382.0	969.5	15.18	2618.9	
1.5	1.0	23.5	2970.2	4.85	1976.8	1.17	1096.8	8.93	2585.8	1023.4	16.23	2816.6	
1.5	1.2	23.7	2995.8	4.87	2038.5	1.17	1133.7	8.97	2594.9	1055.1	16.32	2835.3	
1.5	1.4	23.2	2946.4	4.85	2076.0	1.19	1161.6	8.79	2525.8	1075.5	16.02	2777.6	
Nozzle Expansion													
			P_3. T_3. c_3					**$\bar{P}$. $\bar{T}$. c_3**					
P_1 / atm	**Φ**	**$\frac{P_3}{P_x}$**	**Px / atm**	**Tx / K**	**Ux/ m s^{-1}**	**cx/ m s^{-1}**	**Mx**	**Px / atm**	**Tx / K**	**Ux / m s^{-1}**	**cx / m s^{-1}**	**Mx**	**q / atm**
AR=5.2													
0.5	0.6	34.8	0.07	1091.0	2058.0	650.9	3.16	0.13	1210.9	2147.9	685.7	3.13	0.8
0.5	0.8	30.8	0.09	1408.3	2266.0	743.1	3.05	0.16	1540.5	2351.6	777.2	3.03	0.9
0.5	1.0	30.0	0.10	1596.0	2416.9	802.8	3.01	0.18	1730.6	2499.6	836.0	2.99	0.9
0.5	1.2	30.5	0.10	1586.2	2487.7	822.8	3.02	0.18	1723.5	2574.8	857.7	3.00	0.9
0.5	1.4	32.3	0.09	1491.0	2526.5	823.2	3.07	0.16	1629.3	2621.1	860.6	3.05	0.9
1.0	0.6	34.8	0.14	1079.2	2054.2	648.5	3.17	0.26	1200.3	2145.7	683.9	3.14	1.5
1.0	0.8	31.2	0.18	1388.9	2267.0	739.4	3.07	0.32	1524.2	2355.6	774.6	3.04	1.8
1.0	1.0	30.3	0.20	1590.0	2424.5	802.1	3.02	0.35	1729.1	2510.3	836.4	3.00	1.9
1.0	1.2	30.9	0.19	1570.8	2492.8	820.1	3.04	0.35	1712.8	2583.8	856.4	3.02	1.9
1.0	1.4	33.0	0.18	1464.6	2528.7	817.8	3.09	0.32	1606.9	2627.6	856.6	3.07	1.8
1.5	0.6	35.0	0.21	1071.8	2053.4	646.8	3.17	0.38	1193.3	2145.8	682.5	3.14	2.3
1.5	0.8	31.5	0.27	1377.3	2267.1	737.2	3.08	0.48	1514.3	2357.4	773.0	3.05	2.7
1.5	1.0	30.5	0.29	1586.4	2428.6	801.6	3.03	0.53	1727.9	2516.1	836.6	3.01	2.8
1.5	1.2	31.1	0.29	1560.1	2495.0	818.1	3.05	0.52	1704.7	2588.2	855.2	3.03	2.8
1.5	1.4	33.4	0.26	1448.5	2529.3	814.5	3.11	0.48	1592.8	2630.5	854.1	3.08	2.7
AR=11													
0.5	0.6	95.2	0.03	914.1	2208.7	595.8	3.71	0.05	1014.6	2308.1	627.7	3.68	0.4
0.5	0.8	81.8	0.03	1215.5	2446.8	690.4	3.54	0.06	1329.6	2542.0	722.0	3.52	0.4
0.5	1.0	79.6	0.04	1397.6	2618.8	751.3	3.49	0.07	1515.6	2711.2	782.4	3.47	0.5
0.5	1.2	81.3	0.04	1383.6	2694.1	768.4	3.51	0.07	1503.3	2791.4	801.0	3.48	0.5
0.5	1.4	88.6	0.03	1283.4	2732.3	763.8	3.58	0.06	1402.4	2837.7	798.4	3.55	0.4
1.0	0.6	97.0	0.05	898.0	2205.8	591.5	3.73	0.09	998.8	2307.0	623.8	3.70	0.8
1.0	0.8	83.2	0.07	1192.1	2445.0	685.0	3.57	0.12	1308.2	2543.5	717.6	3.54	0.9
1.0	1.0	80.4	0.07	1386.2	2624.3	748.9	3.50	0.13	1507.4	2720.1	781.0	3.48	0.9
1.0	1.2	82.6	0.07	1362.3	2696.3	763.7	3.53	0.13	1485.4	2797.7	797.5	3.51	0.9
1.0	1.4	91.3	0.06	1251.2	2731.0	755.9	3.61	0.12	1372.8	2841.1	791.8	3.59	0.9
1.5	0.6	97.9	0.08	889.9	2204.3	589.4	3.74	0.14	990.9	2306.4	621.9	3.71	1.1
1.5	0.8	84.1	0.10	1178.4	2443.6	681.9	3.58	0.18	1295.5	2544.0	715.0	3.56	1.4
1.5	1.0	80.9	0.11	1379.4	2627.3	747.4	3.51	0.20	1502.5	2724.9	780.1	3.49	1.4
1.5	1.2	83.4	0.11	1348.3	2696.6	760.6	3.55	0.20	1473.2	2800.4	795.0	3.52	1.4
1.5	1.4	92.8	0.09	1232.0	2729.5	751.1	3.63	0.17	1354.8	2842.1	787.7	3.61	1.3

Table 3. Detonation cycle and nozzle expansion parameters for C_2H_4/air explosive mixture.

C_2H_4/air Explosive Mixture													
CJ Detonation, Taylor Expansion and Mean Pressure of PDE cycle													**T_1 = 298 K**
P_1 / atm	**Φ**	**P_{CJ} / atm**	**T_{CJ} / K**	**M_{CJ}**	**D_{CJ} / m s^{-1}**	**γ**	**c_{CJ} / m s^{-1}**	**P_3 / atm**	**T_3 / K**	**c_3 / m s^{-1}**	**$\bar{P}$ / atm**	**$\bar{T}$ / K**	
0.5	0.6	7.1	2394.3	4.68	1619.6	1.21	917.8	2.69	2015.5	842.1	4.90	2241.4	
0.5	0.8	8.3	2713.9	5.03	1738.9	1.17	964.7	3.14	2353.9	898.4	5.74	2570.0	
0.5	1.0	9.1	2873.3	5.24	1810.0	1.15	996.0	3.41	2518.2	932.4	6.24	2731.9	
0.5	1.2	9.5	2931.2	5.37	1853.2	1.16	1021.0	3.55	2556.7	953.6	6.50	2782.0	
0.5	1.4	9.6	2910.2	5.44	1874.5	1.18	1040.8	3.58	2498.8	964.4	6.58	2745.8	
1.0	0.6	14.2	2403.8	4.69	1622.9	1.22	921.5	5.39	2015.7	843.8	9.82	2247.0	
1.0	0.8	16.8	2747.9	5.06	1748.8	1.17	972.4	6.33	2371.7	903.4	11.56	2597.4	
1.0	1.0	18.4	2922.9	5.28	1823.8	1.16	1005.2	6.90	2552.0	939.3	12.63	2775.1	
1.0	1.2	19.1	2980.5	5.41	1867.0	1.16	1030.9	7.17	2586.9	960.4	13.15	2823.6	
1.0	1.4	19.3	2947.6	5.47	1885.5	1.19	1050.5	7.19	2513.2	970.0	13.24	2773.7	
1.5	0.6	21.4	2408.5	4.70	1624.5	1.22	923.4	8.09	2015.6	844.7	14.73	2249.7	
1.5	0.8	25.3	2766.5	5.08	1754.2	1.18	976.7	9.53	2381.0	906.1	17.41	2612.2	
1.5	1.0	27.7	2951.2	5.31	1831.6	1.16	1010.4	10.42	2571.2	943.1	19.07	2799.7	
1.5	1.2	28.9	3007.9	5.44	1874.6	1.17	1036.6	10.81	2602.9	964.3	19.85	2846.3	
1.5	1.4	29.0	2967.0	5.49	1891.2	1.19	1055.8	10.81	2519.5	972.9	19.92	2787.7	
Nozzle Expansion													
			P_3. T_3. c_3					**$\bar{P}$. $\bar{T}$. c_3**					
P_1 / atm	**Φ**	**$\frac{P_3}{P_x}$**	**Px / atm**	**Tx / K**	**Ux/ m s^{-1}**	**cx/ m s^{-1}**	**Mx**	**Px / atm**	**Tx / K**	**Ux / m s^{-1}**	**cx / m s^{-1}**	**Mx**	**q / atm**
AR=5.2													
0.5	0.6	34.7	0.08	1073.8	1944.2	614.6	3.16	0.14	1194.1	2030.8	648.2	3.13	0.8
0.5	0.8	31.1	0.10	1424.4	2128.5	698.9	3.05	0.18	1555.2	2207.3	730.3	3.02	1.0
0.5	1.0	30.1	0.11	1590.0	2230.0	741.0	3.01	0.21	1725.0	2306.8	771.8	2.99	1.1
0.5	1.2	30.5	0.12	1587.6	2272.0	751.4	3.02	0.21	1727.5	2353.0	783.8	3.00	1.1
0.5	1.4	31.9	0.11	1461.9	2268.0	737.7	3.07	0.21	1606.4	2358.1	773.3	3.05	1.1
1.0	0.6	34.7	0.16	1059.7	1939.3	611.8	3.17	0.28	1181.4	2027.6	646.0	3.14	1.7
1.0	0.8	31.5	0.20	1408.8	2131.5	696.2	3.06	0.37	1542.8	2213.2	728.6	3.04	2.0
1.0	1.0	30.4	0.23	1589.1	2239.3	741.2	3.02	0.42	1728.1	2318.6	772.9	3.00	2.2
1.0	1.2	30.9	0.23	1577.0	2279.0	749.9	3.04	0.43	1721.3	2363.2	783.4	3.02	2.3
1.0	1.4	32.6	0.22	1431.2	2267.8	732.0	3.10	0.41	1579.6	2361.9	769.0	3.07	2.3
1.5	0.6	34.9	0.23	1051.3	1938.0	610.0	3.18	0.42	1173.3	2027.2	644.5	3.15	2.6
1.5	0.8	31.8	0.30	1399.3	2132.9	694.6	3.07	0.55	1535.1	2216.1	727.5	3.05	3.0
1.5	1.0	30.6	0.34	1588.4	2244.6	741.3	3.03	0.62	1729.6	2325.3	773.5	3.01	3.3
1.5	1.2	31.2	0.35	1568.9	2282.4	748.6	3.05	0.64	1715.7	2368.5	782.8	3.03	3.4
1.5	1.4	33.0	0.33	1412.5	2266.9	728.5	3.11	0.60	1562.9	2363.3	766.3	3.08	3.4
AR=11													
0.5	0.6	94.6	0.03	898.9	2085.7	562.3	3.71	0.05	999.6	2181.3	593.0	3.68	0.4
0.5	0.8	83.4	0.04	1233.0	2301.6	650.3	3.54	0.07	1346.3	2389.5	679.4	3.52	0.5
0.5	1.0	79.9	0.04	1393.4	2417.1	693.6	3.48	0.08	1511.6	2502.9	722.5	3.46	0.5
0.5	1.2	81.2	0.04	1384.5	2460.3	701.7	3.51	0.08	1506.5	2550.8	732.0	3.48	0.6
0.5	1.4	86.3	0.04	1253.2	2447.9	683.0	3.58	0.08	1377.0	2548.0	715.9	3.56	0.6
1.0	0.6	96.1	0.06	880.8	2081.3	557.8	3.73	0.10	981.9	2178.8	588.9	3.70	0.8
1.0	0.8	85.0	0.07	1212.9	2302.5	646.0	3.56	0.14	1328.4	2393.4	676.1	3.54	1.0
1.0	1.0	81.0	0.09	1387.0	2425.3	692.4	3.50	0.16	1508.3	2513.8	722.1	3.48	1.0
1.0	1.2	82.8	0.09	1368.0	2465.3	698.4	3.53	0.16	1493.2	2559.2	729.7	3.51	1.1
1.0	1.4	88.6	0.08	1217.4	2444.0	675.1	3.62	0.15	1343.6	2548.5	709.2	3.59	1.2
1.5	0.6	96.9	0.08	871.7	2079.1	555.5	3.74	0.15	972.9	2177.5	586.9	3.71	1.3
1.5	0.8	85.9	0.11	1201.0	2302.6	643.5	3.58	0.20	1317.6	2395.2	674.0	3.55	1.5
1.5	1.0	81.7	0.13	1383.2	2429.9	691.7	3.51	0.23	1506.1	2519.9	721.8	3.49	1.7
1.5	1.2	83.7	0.13	1356.5	2467.5	696.1	3.54	0.24	1483.4	2563.4	727.9	3.52	1.7
1.5	1.4	90.1	0.12	1196.1	2441.1	670.3	3.64	0.22	1323.4	2548.0	705.1	3.61	1.7

5.2.1. Exit velocities

The exhaust gas velocities were calculated through Eq. (1) and appropriate isentropic relations, assuming constant γ and product gas molecular weight, hence, the effect of species changes within the expansion was neglected. The inlet conditions were Taylor expansion ($P_i = P_3$ and $T_i = T_3$) and mean pressure of PDE cycle ($P_i = \overline{P}$ and $T_i = \overline{T}$).

$$U_x = \sqrt{[2\gamma/(\gamma-1)(R/W)T_i][1-(P_x/P_i)^{(\gamma-1)/\gamma}]+c_3^2} \quad (1)$$

Figure 6 displays the nozzle exit velocities at different equivalence ratios for H_2/air and C_2H_4/air steadily-propagating detonations.

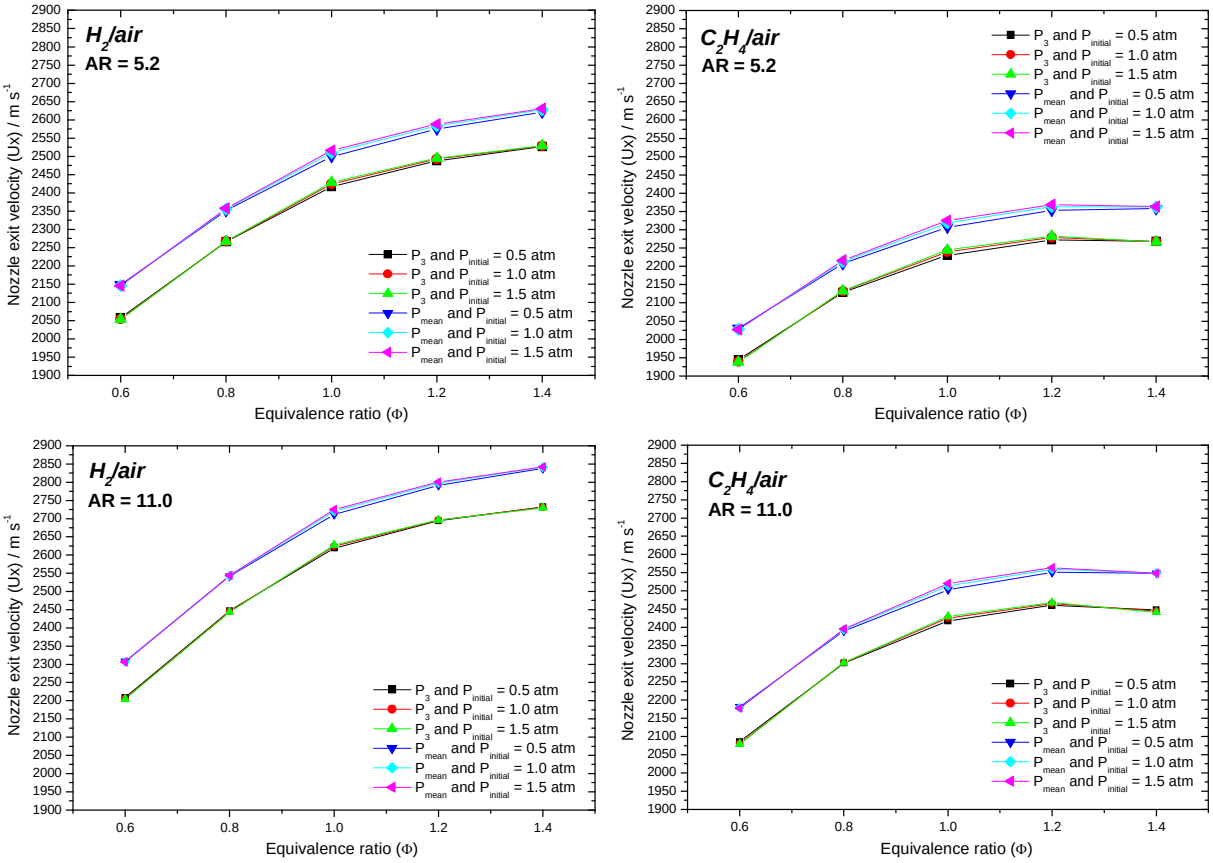

Figure 6. Nozzle exit velocities at different equivalence ratios for H_2/air and C_2H_4/air detonations.

Applying mean pressures of PDE cycle, as nozzle inlet conditions, result in higher exhaust velocities (Fig. 6) and the Mach numbers are equivalent for both H_2/air (Table 1) and C_2H_4/air (Table 2) explosive mixtures. In consequence, the flight pressures and Mach numbers (M_∞) are significantly higher. In this way, flight conditions with static pressures (Px) around of 0.05-0.65 atm, velocities (Ux) of ~2030-2840 m/s and Mach number (Mx) from 3.0 to 3.7 can be experimentally simulated for a PDE.

5.2.2. Flight pressures and Mach numbers

From experimental static pressures (Px) (Tables 2 and 3), the density of air (ρ) was calculated by Atmospheric Calculator software from NASA in correspondent altitude and, consequently, the flight pressures ($P_o(flight) = \rho Ux^2/2$) were established. Considering γ = 1.4, the flight Mach numbers were obtained by Eq. (2).

$$M_\infty = \left\{ \left(\frac{P_o(flight)}{P_o(amb.)} \right)^{\left[\left(\frac{\gamma-1}{\gamma}\right)-1\right]\left[\left(\frac{2}{\gamma-1}\right)\right]} \right\}^{1/2} \quad (2)$$

Flight Mach numbers as a function of flight pressures and altitudes from 0 to 20,000 m are shown in Fig. 7.

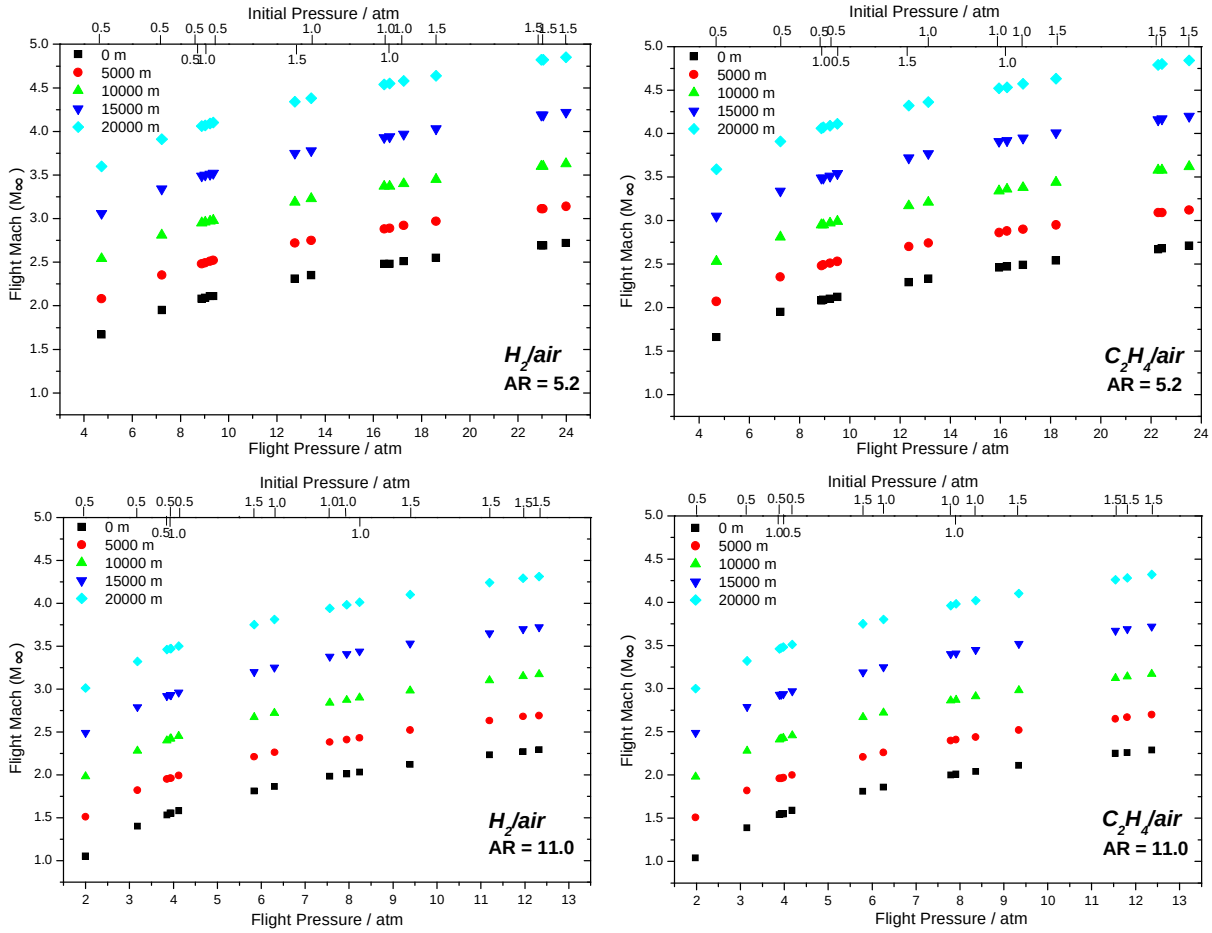

Figure 7. Flight Mach number as a function of flight pressure and altitude for H_2/air and C_2H_4/air detonations at different initial pressures.

The results show supersonic flight regimes using a divergent nozzle with AR = 5.2 (M_∞ = 1.7-4.9) and from transonic to supersonic flight regimes for those with AR = 11.0 (M_∞ = 1.1-4.3) between 0 and 20,000 m of altitude for a PDE device with these initial pressures. However, it is promising to reach higher pressures and velocities through the ignition system proposed here, and, consequently hypersonic flight regimes.

6. CONCLUSIONS

A single-shot pulsed detonation device to simulate PDE combustion conditions was proposed here. A high-voltage nanosecond discharge for PDE ignition systems based on discharge of CO_2 and N_2 lasers through a fast Thyratron switch was developed. Emission images showed high concentration and homogeneous distribution of active species, while Schlieren images revealed the occurrence of semi-spherical shock waves. The results point out streamers discharge or transient plasma with shock wave production, which should be a more effective means to promote shorten DDT or non-thermal ignition.

From 1-D calculations of the parameters of detonation cycle and nozzle expansion for H_2/air and C_2H_4/air explosive mixtures, PDE flight conditions with static pressures around of 0.05-0.65 atm, velocities of ~2030-2840 m/s and Mach number from 3.0 to 3.7 can be experimentally simulated. The results showed a device across the flight regimes from transonic to supersonic. However, it is supposed to achieve hypersonic flight regimes through the efficient ignition system established.

7. ACKNOWLEDGEMENTS

The authors are grateful to Dr. Luiz G. Barreta, Dr. Maria E. Sbampato, Jaime Tsutomu Watanuki and also to Technological Support Division and Prof. Henry T. Nagamatsu Laboratory from IEAv/DCTA. This work was supported by FAPESP (2008/10548-5 and 2009/16385-3) and CNPq (118237/2009-8).

8. REFERENCES

Bertran, C.A., Marques, C.S.T. and Benvenutti, L.H., 1998, "Mapping of Luminescent Species in a Front Flame", Combustion Science and Technology, Vol. 139, No. 1-6, pp. 1-13.

Browne, S., Ziegler, J. and Shepherd, J.E., 2004, "Numerical Solution Methods for Shock and Detonation Jump Conditions", Galcit Report, FM2006.006, pp 1-90.

Cambier, J.L. and Aldeman, H.G., 1995, "The PDWA Concept for Hypersonic Propulsion", Proceedings of the IUTAM Symposium on Combustion in Supersonic Flows, M. Champions and B. Deshaies Eds., Poitiers, France, 12 p.

Cooper, M. and Shepherd, J., 2004, "The Effect of Transient Nozzle Flow on Detonation Tube Impulse", Proceedings of the AIAA/ASME/SAE/ASEE Joint Propulsion Conference and Exhibit, vol. 40, Fort Lauderdale, USA, AIAA-2004-3914.

Dryer, R.S., Kaemming, T.A. and Baker, R.T., 2003, "Reaction Ratio and Nozzle Expansion Effects on the PDE", Proceedings of the AIAA/ASME/SAE/ASEE Joint Propulsion Conference and Exhibit, vol. 39, Huntsville, USA, AIAA-2003-4514.

Falepim, F., Bouchaud, D., Forrat, B., Desbordes, D. and Daniau, E., 2001, "Pulse Detonation Engine Possible Application to Low Cost Tactical Missile and to Space Laucher", Proceedings of the AIAA/ASME/SAE/ASEE Joint Propulsion Conference and Exhibit, Vol. 37, Salt Lake City, USA, AIAA-2001-3815.

FlightGlobal, 5 March 2008, US AFRL Proves Pulse-Detonation Engine Can Power Aircraft. Aircraft Section. 6 September 2008 <http://www.flightglobal.com/articles/2008/03/05/222008/us-afrl-proves-pulse-detonation-engine-can-power-aircraft.html>

Kailasanath, K., 2003, "Recent Developments in the Research on Pulse Detonation Engines", AIAA Journal, Vol. 41, No. 2, pp. 145-159.

Kasahra, J., Takasawa, A, Tanahashi, Y., Chiba, S. and Matsuo, A., "Experimental Investigation of Momentum and Heat Transfer in Pulse Detonation Engines", Proceedings of the Combustion Institute, Vol. 29, Sapporo, Japan, pp. 2847-2854.

Lee, J.H.S., 2008, "The Detonation Phenomenon", 1st Ed., Cambridge University Press, New York, USA, 400 p.

Lee, S.Y., Conrad, C., Watts, J., Woodward, R., Pal, S. and Santoro, R.J., 2000, "Deflagration to Detonation Transition Study using Simultaneous Schlieren and OH PLIF Images", Proceedings of the AIAA/ASME/SAE/ASEE Joint Propulsion Conference and Exhibit", Vol. 36, Huntsville, USA, AIAA-2000-3217.

Lee, S.Y., Watts, J., Saretto, S., Pal, S., Conrad, C., Woodward, R. and Santoro, R., 2004, "Deflagration to Detonation Transition Processes by Turbulence-Generating Obstacles in Pulse Detonation Engines", Journal of Propulsion and Power, Vol. 20, No. 6, pp. 1026-1036.

Marques, C.S.T., 1996, "Distribuição de Espécies Luminescentes em Chamas Explosivas de C_2H_2/O_2", Master Thesis, State University of Campinas, Campinas.

Oliveira, A.C., Minucci, M.A.S., Toro, P.G.P., Chanes Jr., J.B., Myrabo, L.N. and Nagamatsu, H.T., 2008, "Bow Shock Wave Mitigation by Laser-Plasma Energy Addition in Hypersonic Flow", Journal of Spacecraft and Rockets, Vol. 45, No. 5, pp. 921-927.

Oliveira, A.C., Minucci, M.A.S., Toro, P.G.P., Chanes Jr., J.B. and Myrabo, L.N., 2008, "Drag Reduction by Laser-Plasma Energy Addition in Hypersonic Flow", Fifth International Symposium on Beamed Energy Propulsion, Vol. 997, Kailua Kona, USA, pp. 379-389.

Povinelli, L.A., 2002, "Pulse Detonation Engines for High Speed Flight", Nasa Report, TM-2002-211908, pp. 1-8.

Roy, G.D., Frolov, S.M., Borisov, A.A. and Netzer, D.W., 2004, "Pulse Detonation Propulsion: Challenges, Current Status, and Future Perspective", Progress in Energy and Combustion Science, Vol. 30, No. 6, pp. 545-672.

Shiraishi, T., Urushihara, T. and Gundersen, M., 2009, "A Trial of Innovation of Gasoline Engine by Nanosecond Pulsed Low Temperature Plasma Ignition", Journal of Physics D: Applied Physics, Vol. 42, No. 13, 135208.

Starikovskii, A.Yu., 2003, Initiation of Ignition by the Action of a High-Current Pulsed Discharge on a Gas", Combustion, Explosion and Shock Waves, Vol. 39, No. 6, pp. 619-626.

Tangilara, V.E., Dean, A.J., Pinard, P.F. and Varatharajan, B., 2005, "Investigations of Cycle Processes in a Pulsed Detonation Engine Operating on Fuel-Air Mixtures", Proceedings of the Combustion Institute, Vol. 30, Chicago, USA, pp. 2817-2824.

Wintenberger, E.S. and Shepherd, J.E., 1999, "Investigation of Deflagration to Detonation Transition for Application to Pulse Detonation Engine Ignition Systems", Proceedings of the JANNAF Propulsion Meeting, Vol. 16, Cocoa Beach, pp. 1-28.

Zhukov, V.P. and Starikovskii, A.Yu., 2006, "Effect of a Nanosecond Gas Discharge on Deflagration to Detonation Transition", Combustion, Explosion and Shock Waves, Vol. 42, No. 2, pp. 195-204.

9. RESPONSIBILITY NOTICE

The authors are the only responsible for the printed material included in this paper.